Green JOBS

RFCS RESEARCH PROJECT

Leveraging the competitive advantages of end-of-life underground coal mines to maximise the creation of green and quality jobs

Grant Agreement 101057789

Deliverable 3.1

Dense fluids for pumped hydro

European Commission

Research Fund for Coal & Steel

Authors

Aarne Pérez-Bustamante Ilander, Magellan & Barents
Gregorio Fidalgo Valverde, University of Oviedo
Juan José Álvarez Fernández, University of Oviedo
Pedro Riesgo Fernández, University of Oviedo

Deliverable 2.4	
Due date of Deliverable	30.06.2023
Start - End Date of Project	01.07.2022 – 31.12.2025
Duration	3.5 years
Deliverable Lead Partner	Magellan & Barents, S.L.
Dissemination level	Public
Work Package	WP 2
Digital File Name	D3.1 Dense fluids for pumped hydro
Keywords	Dense fluids, energy storage, renewable energy, pumped hydro, unconventional

Disclaimer

The rheometric studies consisting on the determination of the stationary viscous and linear viscoelastic responses of the samples were carried out by Dr. Francisco José Rubio Hernández from the University of Málaga (Spain).

Table of contents

List of Figures

List of Tables

Executive Summary

This deliverable analysis the development of dense fluids required for unconventional pumped hydro by means of using fine coal waste from the three case studies of the project. The characteristic to be sought is a dense fluid with a density higher than three, in order to achieve a yield up to three times that of the conventional pumped hydro.

To achieve this goal, and after preparing the samples for the analysis, rheology studies consisting on determining the stationary viscous and linear viscoelastic responses of the samples were developed, using a MARS III controlled stress rheometer.

The rheometric test was specifically designed to obtain the stationary viscous response of the samples under study. The ability of the samples studied to dissipate and store the energy supplied to them, i.e. the determination of their viscous and elastic components, was obtained by performing an oscillating shear rheometric test (also known as mechanical-dynamic analysis).

The viscoelastic study was carried out to determine the characteristic time of each sample (relaxation time), which gives an idea of the dominant behaviour (viscous or elastic) depending on the duration of the mechanical action exerted on the material behaviour (viscous or elastic) as a function of the duration of the mechanical action exerted on the material.

Also, the pumping capacities of a high-density fluid material using the finite volume method (CFD) were analysed using ANSYS FLUENT software, version 2021 R1, focused on obtaining the mass flow curves as a function of pressure and pumping head and the maximum pumping head.

Finally, and using a sample of the test material, a pumping test was carried out in a lifting tower. The objective was to analyse the viability of this material for various applications in which, in all of them, it is necessary to pump it.

1 Introduction

Work Package No 3, “Deploying circular economy technologies”, mainly aims to analyse the deployment of circular economy technologies for the three case studies based on the valorisation of fine coal waste. Specific objectives are:

1. Assess the development of high-density fluids required for the unconventional pumped hydro.
2. Evaluate the development of soil substitutes to restore waste heaps using different combinations of fine coal waste with other industrial/organic waste.
3. Identify potential approaches for the concentration of mixed rare earth oxides.
4. Analyse the technical specifications, cost data and operational constraints of the selected alternatives for each circular economy technology.
5. Prepare a detailed assessment of the job creation potential of each alternative in terms of production capacity, both for commissioning and operation.

Task 3.1 Dense fluids for pumped hydro, led by M&B with the assistance of UNIOVI, is based on their previous cooperation within unconventional pumped hydro development and with the participation of the three coal mining companies: Węglokoks Kraj S.A. (WEGLO), Hulleras del Norte S.A. S.M.E. (HUNOSA) and Premogovnik Velenje d.o.o. (PV). Specific research was carried out using fine coal waste from the three case studies and suitable additives to develop the high-density fluids needed for the unconventional hydro energy storage system.

Low-density fraction separation by mineralurgical processes, as well as density, fluidity, water/slurry interface and remobilisation tailor-made tests, will be developed at TRL 5 (technology validated in a relevant environment, industrially relevant environment in the case of key enabling technologies) – TRL 6 (technology demonstrated in a relevant environment, industrially relevant environment in the case of key enabling technologies).

The characteristics to be sought for the fluid are a density >3 kg/l, value retention after decommissioning, and 100% recoverable materials. At this density, the yield will be up to three times that of conventional pumped hydro, while the efficiency will be very similar. It will also be checked if the fluid is stable and can be remobilised.

Finally, technical specifications, cost data and operational constraints will be analysed, and a detailed assessment of the job creation potential of each case study in terms of dense fluid production capacity for both commissioning and operation will be prepared.

2 State of the Art

First, we compare the leading energy storage technologies. We intend to store clean energy, so the storage system must also be environmentally benign (Table 2-1).

Table 2-1. Main energy storage technologies

TECHNOLOGY	COST	EFFICIENCY	LIFETIME (CYCLES)	ENVIRONMENTAL IMPACT
H_2	High	25%	?	?
Li-ion	High	70%	4.000	High
Pumped Hydro (conventional)	Very Low	80%	100K+	High
Unconventional Pumped Hydro, M&B	**Low or Very Low[1]**	**80%**	**100K+**	**Low**

[1] It is very competitive when dumpsite materials can be used in an existing cavern.

Because hydropower is a mature technology that has been providing dispatchable power since the very beginning of the electric era, it is the preferred solution for large-scale energy storage, with more than 90% of existing capacity, and it will most likely remain at the top, at least where topographic conditions are good. Conventional pumped hydro requires dams and reservoirs, which take away land for people and wildlife, so several initiatives can be considered unconventional pumped hydro besides Magellan & Barents:

a) Hydrostor

This Canadian company uses water in a surface reservoir to compress air in an underground installation. It is already building commercial projects. Using a dense fluid would allow two or three times the power and energy storage capacity they achieve with water. https://www.hydrostor.ca/. The opportunities for synergies are considerable, particularly in their more advanced projects (Figure 2-1).

b) Pyhäsalmi

The Pyhäsalmi energy storage project is a 75 MW/530 MWh project in a mine about 1450 meters deep. It got EUR 26.3 million from the Government of Finland in 2022 (Figure 2-2). The Pyhäsalmi project is exciting because it is developing high-head hydropower equipment very similar to our needs, with an excellent opportunity to share development and production costs. https://www.epv.fi/en/project/a-pump-storage-station-for-pyhasalmi-mine/. There are exciting overlaps; we are very interested in their ultra-high-head Pelton turbines, and can probably contribute to our water-tight solutions.

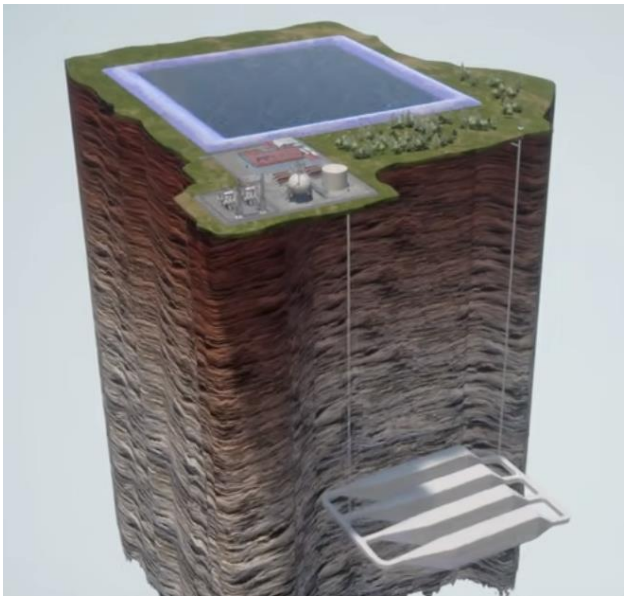

Figure 2-1. Scheme of Hydrostor

Figure 2-2. Scheme of Pyhäsalmi

c) Rheenergise

RheEnergy uses a dense fluid likely made from magnetite fines and water. The density is 2.5, which can be easily achieved (Figure 2-3). The company claims the reduction in tank or reservoir volume and associated civil works as their main advantage. https://www.rheenergise.com/

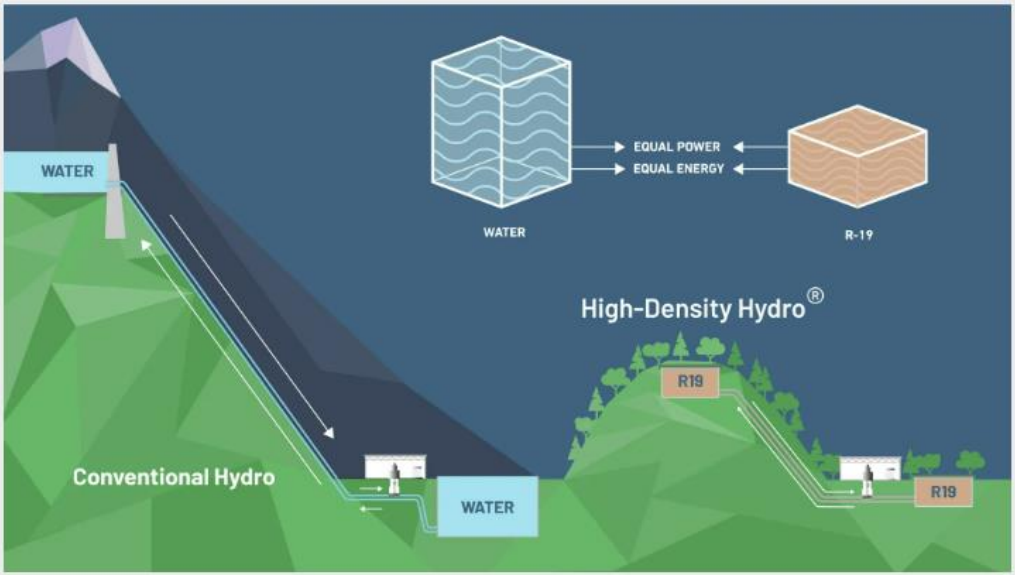

Figure 2-3. Scheme of Rheenergise

d) Shell International

Shell prepared and patented a project in The Netherlands, EP0191516A1, but the project was cancelled after the 1986 Chernobyl NPP accident. It could not use any escarpments, so it needed two underground reservoirs for dense fluid (Figure 2-4). https://patents.google.com/patent/US4691524

These projects point to a diverse, disruptive, relatively mature technological field, attracting multimillion Euro investments in several countries. Typically for any R+D ecosystem, M&B's technology acts as a force multiplier for some of those projects and benefits from specific developments by others.

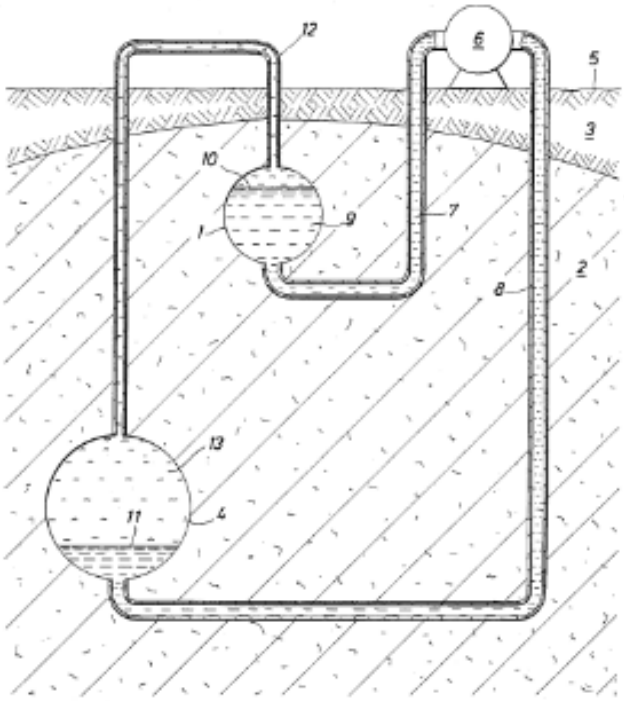

Figure 2-4. Scheme of Shell International

3 Unconventional pumped hydro storage characteristics

Renewable energies, such as those harnessed from the sun, wind and water, are popular forms of energy to generate electricity since they have minimal impact on our environment. For example, renewable energy does not pollute the environment such as CO_2 emissions.

Although renewable energy has advantages, there are also disadvantages. For example, renewable energy is highly dependent on nature, which is undependable or unreliable. Solar power requires sunlight, which can be affected by clouds; wind power relies on the wind, which can come and go; water power relies on water, which relies on a limited number of waterways and has numerous challenges. This unreliability or inconsistencies of renewable energy contribute to imbalances in supply and demand. Such imbalances cause huge swings in energy pricing.

Conventional pumped hydro energy relies on water flowing from an upper reservoir to a lower reservoir through a penstock. The water then turns into a turbine to generate electricity sent to the grid. Water is pumped up the penstock to recharge the upper reservoir. Pumped hydro energy storage, since it has, besides a turbine, a pump to recharge the system, provides controllability and reliability. This stabilises the imbalances of supply and demand, which are inherent in traditional renewable energy sources.

Furthermore, an essential consideration for conventional hydropower energy systems and pumped hydro storage is the footprint required by the reservoirs.

Unconventional pumped hydro storage is directed to a small footprint pumped hydro energy storage system and method with high power output.

Embodiments generally relate to an unconventional pumped hydro storage system and application of the pumped hydro storage system. The system has a smaller footprint and higher energy density than conventional pumped hydropower energy systems.

The system uses a high-density fluid and allows for different configurations where upper and lower reservoirs may be at the same elevation. Hydraulic pumps and turbines may be placed higher than the lower reservoir, for example, on the surface above an underground mine.

In particular, an embodiment relates to a pumped hydro storage system, which includes a first and second reservoir, disposed below the first reservoir. The system also includes a turbine unit. The turbine unit includes a first turbine unit flow port and a second turbine unit flow port.

A penstock is provided in fluid communication with the first and the second reservoirs. The penstock includes a first portion coupled to the first reservoir, the first turbine unit

flow port, and a second portion coupled to the second reservoir and the second turbine unit flow port.

The turbine unit is disposed of proximate to the second reservoir. A slurry circulates through the system. The slurry is a high-density fluid which has a density greater than water. The slurry flows through the turbine in a first or forward direction from the first reservoir to the second reservoir to cause the turbine unit to generate energy.

In the recharge mode, the slurry flows through the turbine unit in the second or reverse direction from the second reservoir to the first reservoir to recharge the system. The high-density slurry increases the system's power output compared to water systems.

The lower-density fluid flowing into the lower reservoir causes the turbine to turn in the first direction, generating power. To recharge the system, the pump pumps the lower-density fluid down to the cavity tank in the second direction, causing the high-density fluid to flow back into the upper reservoir.

Providing the high-pressure cavity tank below ground is advantageous as it can utilise the lithostatic pressure, thereby countering the pressure caused by the fluid. This reduces the construction costs of the lower reservoir. In addition, the mountain terrain provides a natural elevation for the upper reservoir. The height at which the upper reservoir is elevated can be configured based on output requirements. For example, lower elevations may be helpful to reduce costs associated with building the upper reservoir and penstock if output requirements are met.

The fluid of the pumped hydro storage system is a high-density fluid. The high-density fluid has a density greater than water. For example, the high-density fluid may have a density of> 3x, where x is the density of water. In one embodiment, the high-density fluid is a slurry mixture.

Various types of slurry mixtures may be employed. The slurry mixture may include, for example, metal oxide particles mixed with a lower-density fluid, such as water.

Other types of particles and lower-density fluids may also be helpful. The volume of particles in the slurry may equal or exceed 50%.

For example, the percentage of particles may be about 50 -85%. In other embodiments, the percentage of particles may be 50 - 75%. The higher the volume of particles, the higher the density of the slurry. All percentages are volume percentages. Other percentages may also be helpful.

A small surfactant may be added to prevent the slurry from coalescing and improve flow. For example, less than 1% of surfactant can be added. In some cases, antifreeze may be added to prevent freezing of the slurry. The concentration of antifreeze should be sufficient to prevent the slurry from freezing.

An example of a high-density fluid is a magnetite slurry mixture. The magnetite slurry

mixture may achieve a density of 3 to 4 tons/m, more than 3 times the density of water. Other types of slurry mixtures, as discussed, can also be employed as high-density fluid. The density may depend on the mineral content and composition.

A more compact pumped hydro energy storage system can be achieved by employing high-density fluid. For a given reservoir or tank volume, the energy storage capacity is proportional to the density of the fluid. For example, in the case where the high-density fluid has a density of 3x, the energy storage capacity of the system is 3 times that when water is used. This is because the mass flow rate is about 3 times more than water's.

Alternatively, the system can produce the same energy output using less fluid volume and a lower height differential between the upper and lower reservoirs. This results in lower costs and more flexibility in designing a system to satisfy output requirements.

An advantage, as discussed with using a high-density fluid, is higher power output. A high-density fluid can be easily retrofitted into existing pumped hydro storage systems by modifying the penstock and pump to handle the high-density fluid, thereby increasing the power output. Furthermore, existing designs of hydro storage systems can be modified to serve as models for highly efficient hydro storage systems which handle a high-density fluid. The cost to build, for a given power output requirement, would be reduced due to less volume needed, smaller penstocks and reduced elevation or height between the reservoirs.

4 Treatment of samples for initial analysis

This section will describe the procedure for preparing samples for initial analysis in an accredited laboratory. Two samples have been taken from company Hulleras del Norte S.A. S.M.E. (HUNOSA - Spain), one sample from company Węglokoks Kraj S.A. (WEGLO - Poland) and one sample from company Premogovnik Velenje d.o.o. (PV - Slovenia).

It is necessary to point out that in the case of HUNOSA, some samples have been taken since the El Batán coal preparation plant only carries out a pre-treatment by screening the material from the San Nicolás well, the company's only active mine.

To compare, two samples have been taken, one from the El Batán coal preparation plant and another from the old coal preparation plant tailings accumulated in the La Matona dump. Five bags of between 20 and 25 kg of material were taken from the El Batán coal preparation plant and as many from the La Matona dump.

4.1 Sample drying procedure and humidity calculation

The procedure, using the UNE 32-001-81 Standard, for drying the sample at laboratory temperature and calculating the **imbibition humidity (X)** was as follows:

- Place the material from a sample bag in an appropriate number of large trays, with a volume between 0.015m^3 (0.50m x 0.30m x 0.10m) and 0.013m^3 (0.51m x 0.34m x 0.075m), so that it dries in a time of approximately one or two weeks. Between 5 and 10 kg of the sample will be placed per tray.
- The quantity of 1 and 3 kg of sample is taken in a smaller tray, with a volume of 0.004m^3 (0.30m x 0.24m x 0.055m), to determine imbibition humidity.
    - The empty tray is weighed (P_1), and its value is recorded.
    - The tray with the sample is weighed again (P_2).
    - The weight of the empty tray is subtracted, and the weight of the sample (P_3) is obtained.

$$P_3 = P_2 - P_1$$

- It is left to dry at laboratory temperature until the weight stabilises, checking every 3 days the variation in weight in grams and calculating the percentage of humidity lost. This process can take approximately 1-2 weeks.
- Once the weight stabilises, the imbibition humidity is obtained.

The procedure, using the UNE 32-001-81 Standard, for drying the sample in a laboratory drying oven and calculating the **hygroscopic humidity (M)** was as follows:

- An empty tray is weighed, and its value is noted (m_2).
- The empty tray is placed in the oven at a temperature between 378 and 383 K (105 and 110ºC), its air atmosphere is renewed 3 to 5 times per hour, and it is weighed again when hot, noting its new value (m_4).

- The sample from the imbibition humidity is placed in the tray and distributed evenly over the entire surface (maximum 1 g/cm^2). The tray plus the sample (m_1) is weighed and placed in the oven to dry.
- It is kept at that temperature until constant mass. The drying time ranges between 3 and 6 hours.
- Once the weight of the tray plus the hot sample has stabilised, it is taken to the balance and its value (m_3) is recorded.
- The hygroscopic humidity of the analysed sample is obtained employing the following expression:

$$M = \frac{(m_1 - m_4) - (m_3 - m_2)}{(m_1 - m_4)}$$

m_1 = mass, in grams, of tray and sample as received
m_2 = mass, in grams, of the empty tray
m_3 = mass, in grams, of tray and sample after heating
m_4 = mass, in grams, of the empty, dry tray

When the sample, as in this case, has been air-dried, the **total humidity (H_T)**, in percentage, is calculated using the following formula:

$$H_T = X + M\,(1 - (X / 100))$$

X = Imbibition humidity in per cent
M = Hygroscopic humidity in per cent

4.2 Sample grain reduction procedure

Next, once dry, the procedure used to reduce the grain of the samples to obtain an optimal size will be described.

The machines used are the following:

- Single-acting jaw crusher (Figure 4-1, left).
- Disc mill (Figure 4-1, right)
- Jones or channel sampler (Figure 4-2).
- Scales (Figure 4-2).

Figure 4-1. Single-acting jaw crusher and Disc mill

Figure 4-2. Jones or channel sampler for coarse and fine

Figure 4-3. Scales

Initially, the machines must be cleaned to eliminate any impurities from previous procedures that could contaminate the samples. Initially, the sample is passed through the jaw crusher, which crushes it, giving it a maximum size of 2 cm, optimal for introducing it into the disc mill, which reduces it to a maximum size of 5 mm. Once this size has been achieved, the desamplers will be used to obtain the appropriate sample size for analysis.

4.2.1 Sample from the La Matona dump (HUNOSA)

Next, the drying procedure of the sample extracted from the La Matona of the HUNOSA dump will be described. Figure 4-4 shows the state of the La Matona sample.

Figure 4-4. Initial state of the La Matona sample

Initially, one of the bags, of approximately 20 kg of the sample, was placed in two large trays with a volume of 0.015m^3 each and the amount of 2526.60 g in another small tray, 0.004m^3, which weighs 551.50 g when empty, as seen in Figure 4-4. After 4 days, the small tray was weighed again, after eight days it was weighed again, verifying that the weight had not yet stabilised. After 12 days, the same operation was carried out, observing the final stabilised weight and being able to obtain the imbibition humidity of the 12.6%. The results obtained are those presented in the following table (Table 4-1):

Table 4-1. Variation in the weight of the La Matona sample and calculation of imbibition humidity

DATE	WEIGHT (g)		VARIATION	
	Sample+tray	Sample	g	%
28/02/2022	3075.10	2523.60	0.00	0.00%
04/03/2022	2830.40	2278.90	-244.70	-10.70%
07/03/2022	2792.10	2240.60	-38.30	-1.70%
09/03/2022	2787.70	2236.20	-4.40	-0.20%
11/03/2022	2787.70	2236.20	0.00	0.00%
		TOTAL VARIATION:	-287.40	-12.6%

Before placing the sample in the tray for humidity calculation, it was placed in the oven at a temperature between 378 and 383 K (105 and 110ºC) and said tray was weighed once dry, obtaining a value of 550.7g. This value is obtained to calculate the hygroscopic humidity, which turned out to be 0.9% once the formula was applied. The values used for the calculation are detailed in Table 4-2.

Table 4-2. Calculation values of hygroscopic humidity in the sample of La Matona

CONCEPT	SYMBOL	MASS (g)
Initial mass in grams of tray + sample	m_1	2787.7
Mass in grams of the initial empty tray	m_2	551.5
Mass in grams of tray + sample after heating	m_3	2768.3
Mass in grams of an empty and dry tray	m_4	550.7

Once the imbibition and hygroscopic humidity are obtained, the **total humidity** is obtained, which turns out to be 13.4%.

Next, once the sample was dry, it was passed through the jaw crusher, obtaining the optimum size for the disc mill. Figure 4-5 shows the different machines through which the La Matona sample was passed and the grain size obtained in the jaw crusher.

Figure 4-5. Grinding treatment of the La Matona sample

After grinding the material, it is passed through the large desampler and the finer one to obtain a sample bag for analysis (Figure 4-6).

Figure 4-6. Final sample of La Matona

4.2.2 Sample from the El Batán dump (HUNOSA)

Next, the drying procedure of the sample extracted from the El Batán coal preparation plant of HUNOSA will be described. Figure 4-7 shows the state of the El Batán sample.

Figure 4-7. The initial state of the El Batán sample

Initially, one of the bags, of approximately 25 kg of the sample, was placed in four large trays with a volume of 0.013m^3 each and the amount of 1357.80g in another small tray, 0.004m^3, which weighs 565.50g when empty, and as seen Figure 4-7. After four days, the small tray was weighed again. After eight days, it was weighed again, verifying that the weight had stabilised and obtained an imbibition humidity of 6.16%. The results obtained are those presented in the following Table 4-3.

Table 4-3. Weight variation of the El Batán sample and imbibition humidity

DATE	WEIGHT (g)		VARIATION	
	Sample+Tray	Sample	g	%
28/02/2022	1923.30	1357.80	0.00	0.00%
04/03/2022	1845.20	1279.70	-78.10	-6.10%
07/03/2022	1844.50	1279.00	-0.70	-0.05%
09/03/2022	1844.70	1279.20	0.20	0.02%
11/03/2022	1844.50	1279.00	-0.20	-0.02%
	TOTAL VARIATION:		-78.80	-6.16%

Before placing the sample in the tray for humidity calculation, it was placed in the oven at a temperature between 378 and 383 K (105 and 110ºC) and said tray was weighed once dry, obtaining a value of 564.7g. Once the formula was applied, this value was obtained to calculate the hygroscopic humidity of 0.6%. The values used for the calculation are in Table 4-4.

Table 4-4. Calculation values of hygroscopic humidity in a sample from El Batán

CONCEPT	SYMBOL	MASS (g)
Initial mass in grams of tray + sample	m_1	1844.5
Mass in grams of the initial empty tray	m_2	565.5
Mass in grams of tray + sample after heating	m_3	1840.7
Mass in grams of an empty and dry tray	m_4	564.2

Once the imbibition and hygroscopic humidity have been obtained, the **total humidity** is obtained, which turns out to be 6.6%.

Next, once the sample was dry, it was passed through the jaw crusher, obtaining the optimum size for the disc mill. In Figure 4-8, you can see the difference in the grain size of the sample passed through the jaw crusher and after passing it through the disc mill.

Figure 4-8. Grinding treatment of the El Batán sample

After grinding the material, it is passed through the large sampler and the finer one to obtain a sample bag for analysis (Figure 4-9).

Figure 4-9. Final sample of La Matona

4.2.3 Sample from the WEGLO dump

Next, the drying procedure of the sample extracted from WEGLO will be described. Figure 4-10 shows the state of the WEGLO sample.

Figure 4-10. The initial state of the WEGLO sample

In this sample, it was not necessary to calculate the moisture content because it was scorched, and there was no variation in weight.

Next, the sample was passed through the disc mill, obtaining the optimum size for the analysis.

After grinding the material, it is passed through the large sampler and the finer one to obtain a sample bag for analysis.

4.2.4 Sample from the PV dump

Next, the drying procedure of the sample extracted from PV will be described. Figure 4-11 shows the state of the VP sample from Slovenia.

Figure 4-11. The initial state of the VP sample

Initially, one of the bags, of approximately 25 kg of the sample, was placed in 3 large trays with a volume of 0.013m^3 each and 518,3g in another small tray, 0.004m^3, which weighed 567.10g. After three days, the small tray was weighed again. After seven days, it was weighed again, and the same after 14 days verifying that the weight had already stabilised and obtained imbibition humidity of 6.16%. The results obtained are those presented in the following Table 4-5.

Table 4-5. Weight variation of the El Batán sample and imbibition humidity

DATE	WEIGHT (g)		VARIATION	
	Sample+Tray	Sample	g	%
21/02/2023	1085.40	518.30	0.00	0.00%
24/02/2023	1031.80	464.7	-53.60	-10.34%
28/02/2023	1031.00	463.9	-0.80	-0.17%
14/03/2023	1031.00	463.9	0.00	0.00%
		TOTAL VARIATION:	-78.80	-10.51%

Before placing the sample in the tray for humidity calculation, it was placed in the oven at a temperature between 378 and 383 K (105 and 110ºC) and said tray was weighed once dry, obtaining a value of 565.7g. This value is obtained to calculate the hygroscopic humidity, which turned out to be 3.7% once the formula was applied. The values used for the calculation are in Table 4-6.

Table 4-6. Calculation values of hygroscopic humidity in a sample from El Batán

CONCEPT	SYMBOL	MASS (g)
Initial mass in grams of tray + sample	m_1	1028.6
Mass in grams of the initial empty tray	m_2	567.1
Mass in grams of tray + sample after heating	m_3	1012.7
Mass in grams of an empty and dry tray	m_4	565.7

Once the imbibition and hygroscopic humidity have been obtained, the **total humidity** is obtained, which turns out to be 13.1%.

Next, once the sample was dry, it was passed through the disc mill, obtaining the optimum size.

4.2.5 Samples for Dense Fluids

Four 150 g samples with a grain size <0.1 mm were taken for the dense fluid and viscosity tests. The samples were labelled as shown in Figure 4-12:

- FD-ESL for the PV sample (Slovenia)
- FD-PO for the WEGLO sample (Poland)
- FD-MA for the La Matona sample (HUNOSA-Spain)
- FD-BA for the El Batán sample (HUNOSA-Spain)
- FD-PT-1 for one of the control standards
- FD-PT-2 for one of the other control standards

Figure 4-12. Samples for Dense Fluid and Viscosity Tests

5 Results of the rheology test

The object of the Rheometric studies consisted of determining the stationary viscous and linear viscoelastic responses of six samples. Dr Francisco José Rubio Hernández carried it out from the University of Málaga (Spain).

5.1 Rheometer

A MARS III controlled stress rheometer (Thermo-Haake, Germany) was used. (Figure 5-1). The span geometry is the one best suited to the characteristics of the samples supplied (Barnes & Carnalli, 1990). Figure 5-2 shows a picture of the span geometry and its dimensions. The spacing between the rotor and stator complied with the single shear condition (R!=1,2R"). The spacing between the rotor and the bottom of the outer cylinder was four mm, complying with the condition that this distance is equal to or greater than ten times the particle size (0.1 mm) present in the problem fluid.

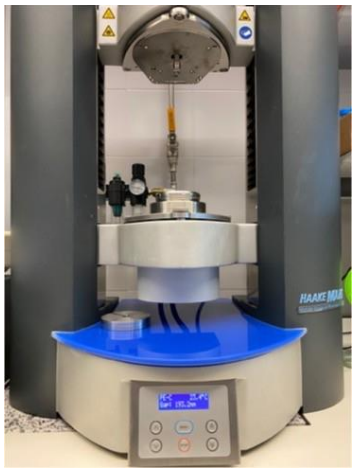

Figure 5-1. Controlled stress rheometer Haake MARSIII.

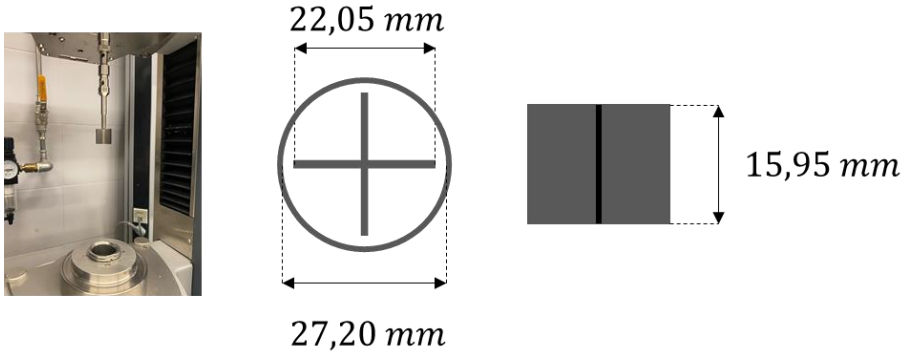

Figure 5-2. The geometry of spans.

5.2 Rheometric test

Figure 5-3 describes the rheometric test specifically designed to obtain the stationary viscous response of the samples under study. After a conditioning phase of the sample after being placed in the span geometry, a decreasing sequence of logarithmically distributed shear velocities (velocity gradient) is applied. The measured magnitude is the stress the specimen opposes to the rotation in the same shear direction. The accepted value for each shear rate ($\dot{\gamma}$) is the stationary stress (τ), accepting as such the value that shows a variation of less than 1% for ten s.

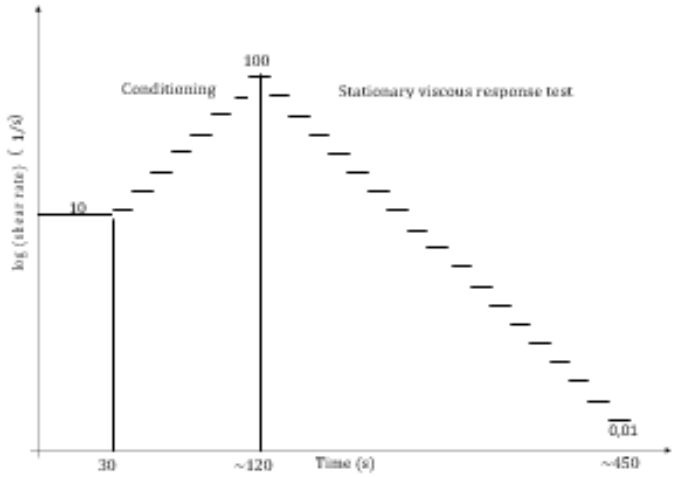

Figure 5-3. The test was designed to study the stationary viscous response.

The apparent viscosity (η) of the sample, corresponding to each shear rate, is calculated from its definition,

$$\eta = \frac{\tau}{\dot{\gamma}} \qquad (1)$$

In the case of a Newtonian fluid, this viscosity, for a given temperature and pressure, will be constant. However, when the viscosity depends on the shear rate, i.e. $\eta = \eta(\dot{\gamma})$, the fluid will be non-Newtonian. It should be noted that there are other reasons why a fluid may be non-Newtonian (viscosity dependence on time or the fluid's ability to store energy). The test described in Figure 3 was designed to determine the dependence $\eta = \eta(\dot{\gamma})$.

The ability of the samples studied to dissipate and store the energy supplied to them, i.e. the determination of their viscous and elastic components, was obtained by performing an oscillating shear rheometric test (also known as mechanical-dynamic analysis),

$$\gamma = \gamma_0 \, sen \, \omega t \qquad (2)$$

where γ is the shear strain applied to the sample, γo is the maximum value of this strain, and ω is the angular frequency of the oscillation ([F.J. Rubio Hernández, Flujos no-Newtonianos y Reología, UMA Editorial, Universidad de Málaga, Málaga 2022]. The test consists of two parts. First, an amplitude sweep is performed on the deformation of the specimens, starting from a minimum value and increasing logarithmically in value while keeping the oscillation frequency constant (Figure 5-4).

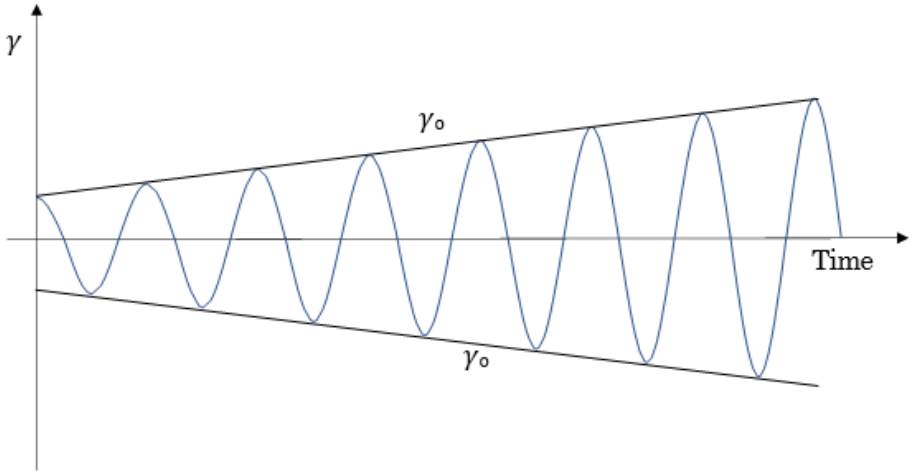

Figure 5-4. Amplitude sweep. The first part of the test was designed for the viscoelastic study of the samples.

In this way, we can determine the value of γo that, at most, we can apply to the sample so that the microstructure it develops in the resting state responds linearly. In other words, whenever we study the response of the fluid in this region, it will be of the type,

$$\tau = \tau_o \, sen \, (\omega t + \varphi) \qquad (3)$$

where τo is the maximum stress supported by the fluid when a maximum deformation γ_o is applied, and φ is the phase difference between the harmonic signals given by (2) and (3).

Once the maximum value of the amplitude γom has been obtained, we proceed to the second part of the mechanical-dynamic analysis. In this case, keeping the oscillation amplitude below the value γom, a frequency sweep is performed (Figure 5-5). In this way, we will be able to know which component (viscous or elastic) of the viscoelastic response of the fluid dominates and in what proportion when carrying out short (high frequencies) or long-lasting (low frequencies) tests. The frequency value corresponds to a 50% split of both components of the viscoelastic response, and, more appropriately, the resulting time value is a characteristic parameter of the material (relaxation time). The viscous and elastic components are obtained from the development of the trigonometric function (3),

$$\tau = \tau_o \cos \varphi \, sen \, \omega t + \tau_o \, sen \, \varphi \cos \omega t \qquad (4)$$

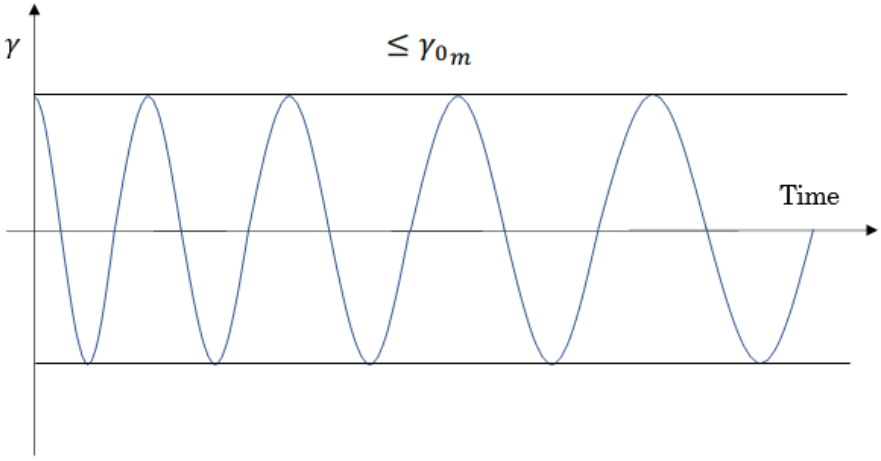

Figure 5-5. Frequency sweep. The second part of the test was designed for the viscoelastic study of the samples

The first summand corresponds to the part of the stress in phase with the strain, i.e. it results from the elastic component of the fluid, while the second summand is in phase with the strain rate ($\dot{\gamma} = \gamma o \omega cos\omega t$), i.e. it results from the viscous component of the fluid. Consequently, two new rheological parameters are defined to quantify both components,

$$G' = \frac{\tau_0}{\gamma_0} cos\varphi$$
$$G'' = \frac{\tau_0}{\gamma_0} sen\varphi \quad (5)$$

While G' gives an idea of the elasticity of the fluid (elastic modulus), the value of G'' gives the importance of the viscous response of the fluid (viscous modulus).

5.3 Results

The experimental results show an average of at least three measurements in each case. A precondition for fluid under rheometric study is that it must be homogeneous. Since the samples presented a specific coagulation state upon receipt (Figure 5-6), they were manually shaken for at least 5 minutes before starting the rheometric studies. The reproducibility of the obtained rheometric results confirmed that the samples' homogeneity was achieved this way.

Figure 5-6. The initial physical state of samples in the AMU rheology laboratory

5.4 Viscous response

The apparent viscosity curves are shown in Figure 5-7. In all cases and in the range of shear rates that were accessible (reproducible results), the viscosity decreases with increasing shear rate. This is the non-Newtonian behaviour known as rheo-fluidising (shear-thinning).

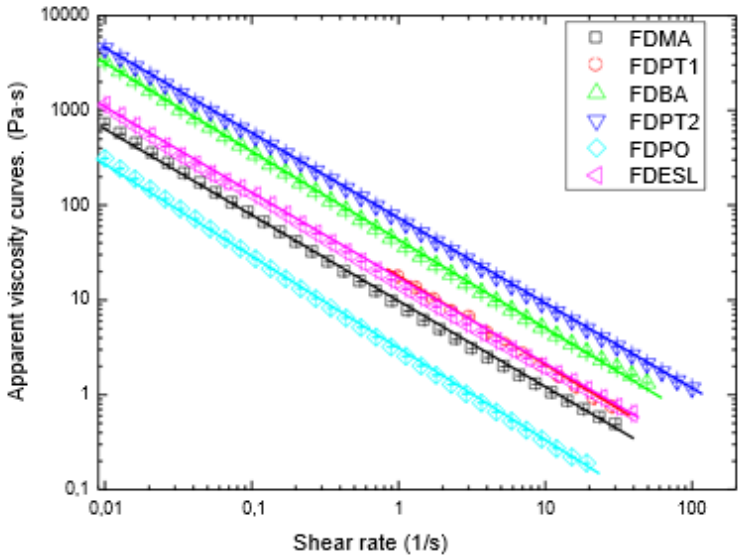

Figure 5-7. Apparent viscosity curves

The experimental results are presented in Appendix 1 and conform, in all cases, to a power law (Ostwald-de Waele),

$$\eta = K\dot{\gamma}^{n-1} \qquad (6)$$

Where K is the consistency index (Pa - sn), and n is the flow index (dimensionless).

Table 5-1 shows the values of these parameters, as well as the correlation coefficient (r^2) corresponding to each fit of the experimental points with equation (6).

Table 5-1. Parameters resulting from the power-law fit

SAMPLE	K ($Pa \cdot s$)	n (-)	r^+	η . ($Pa \cdot s$)
FDPO	3.0 ± 1.0	0.011 ± 0.004	0.9995	3.2 ± 0.1
FDMA	9.5 ± 1.0	0.076 ± 0.004	0.9993	9.6 ± 0.1
FDESL	15.5 ± 1.0	0.093 ± 0.004	0.9994	16.7 ± 0.1
FDPT1	17.3 ± 1.0	0.049 ± 0.009	0.9989	19.0 ± 0.1
FDBA	42.5 ± 1.0	0.073 ± 0.003	0.9995	43.5 ± 0.1
FDPT2	70.5 ± 1.0	0.102 ± 0.001	0.9999	73.8 ± 0.1

Since the flow index values for each sample are different, varying even by order of magnitude, a comparison based on the consistency index is impossible since the units are different in each case (Pa - sn). However, taking into account that when the shear rate is 1 $^{S-1}$ $log\dot{\gamma}$=0, we can use the viscosity value corresponding to this shear rate value as a valuable parameter to compare the viscous responses of the six samples supplied (Naranjo-Herrera, 2022).

Thus, we will conclude that the viscous response of the samples follows the increasing order,

FDPO < FDMA < FDESL < FDPT1 < FDBA < FDPT2 (7)

5.5 Viscoelastic response

The viscoelastic study was carried out to determine the characteristic time of each sample (relaxation time), which gives an idea of the dominant behaviour (viscous or elastic) depending on the duration of the mechanical action exerted on the material behaviour (viscous or elastic) as a function of the duration of the mechanical action exerted on the material. This study is defined in the linear viscoelastic response region. This is why an amplitude sweep was applied (Figure 5-4), obtaining the results shown in Figure 5-8. These experimental results are presented in Appendix 2,

FDPO < FDMA < FDESL < FDPT1 < FDBA < FDPT2 (8)

Which, moreover, confirms the goodness of sequence obtained from the purely viscous response (7).

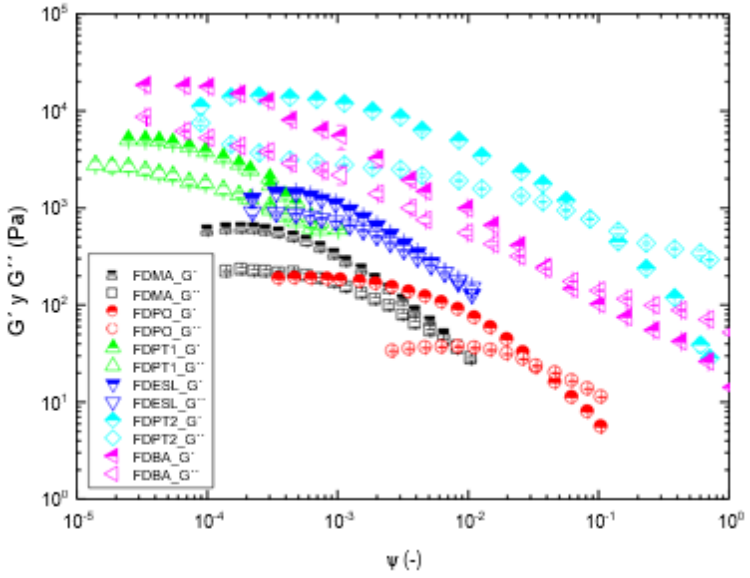

Figure 5-8. Amplitude sweeps corresponding to the six samples studied

The dominant response of the substances when subjected to tests of different durations was determined after obtaining the corresponding maximum amplitude values delimiting the respective regions of linear viscoelastic and non-linear viscoelastic behaviour. This information is obtained from the results obtained with the so-called frequency sweep test (Figure 5-5). Figure 5-9 shows the results of the frequency sweeps in the region of linear viscoelastic behaviour. These experimental results are presented in Appendix 3. The inverse of the frequency value where both viscoelastic moduli coincide is used as the characteristic time of the material. When the duration of the mechanical action exerted on a sample is less than this

characteristic time, its response will be closer to that of a solid.

In contrast, the response will be reminiscent of that of a liquid when the duration of the mechanical action is greater than the characteristic time of the material. In either case, the responses are, strictly speaking, viscoelastic. This characteristic time indicates the influence of the duration time of the mechanical action on the dominance of one or the other viscoelastic component. According to the results in Figure 5-9, the characteristic times (indicated in the exact figure) follow the increasing order,

$$FDPT1 < FDESL < FDMA < FDBA < FDPO < FDPT2 \qquad (9)$$

For the FDPT2 sample, due to the experimental limitation, we could only conclude that its relaxation time will be higher than 1000 s

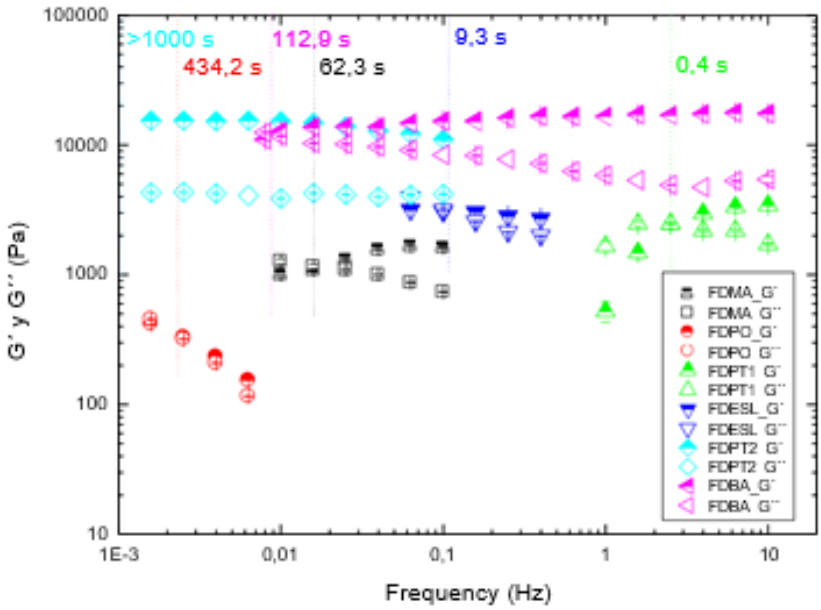

Figure 5-9. Amplitude sweeps corresponding to the six samples studied

6 Report of fluidity in test installation with h=40 m

Magellan & Barents has asked the IDONIAL Foundation to analyse the pumping capacities of a high-density fluid material using the finite volume method (CFD). A sample of the test material was used, and a pumping test was carried out in the lifting tower owned by IDONIAL, located in GIJON.

The objective is to analyse the viability of this material for various applications in which, in all of them, it is necessary to pump it.

Initially, laboratory tests were carried out to obtain the plastic properties of the fluid, which were subsequently used in the simulation.

The analyses, by the finite volume method using ANSYS FLUENT software, version 2021 R1, focused on obtaining the mass flow curves as a function of pressure and pumping head and the maximum pumping head. For this purpose, the following studies and the subsequent post-processing of results were carried out:

- **Analysis 1 - Study of the maximum pumping head.** This study was carried out by applying an inlet pressure on the fluid inside a pipe of virtually infinite length. The equilibrium height of the fluid was established for different pressures.
- **Analysis 2 – Mass flow study.** This study was carried out by applying an inlet pressure to the fluid inside a pipe of a given length. The outlet flow rates were measured for the different combinations of pressure and length.

The rheological characterisation of the high-density fluid material under study is necessary for the abovementioned analyses. This characterisation was carried out employing laboratory tests.

6.1 Material properties

Laboratory rheological tests were carried out on the sample to characterise the high-density fluid under study. The density and plastic properties of the material were determined, and flow curves were obtained to determine the variation of the viscosity of the material as a function of shear rate.

A 10 ml test tube was used to measure the density, flush with the material under study, obtaining a value of 2.180 mg/ml.

On the other hand, the graph in Figure 6-1 shows the values obtained from the rheological test. The material has a pseudo-plastic behaviour with thixotropic properties, i.e. the viscosity is time-dependent, especially at low speeds.

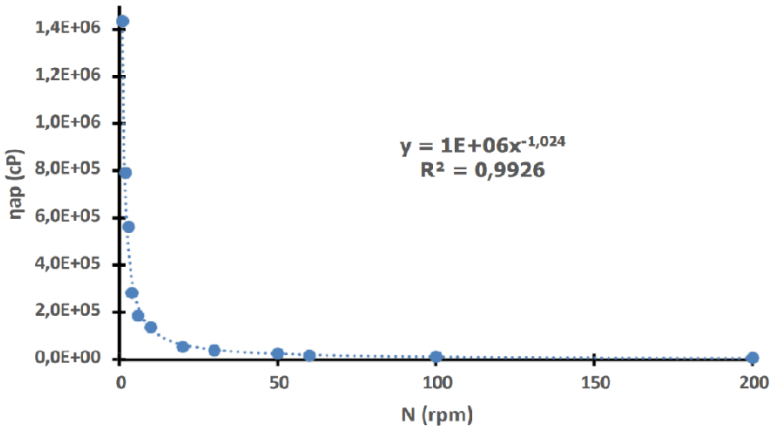

Figure 6-1. Viscosity of the material

The resulting curve is fitted with an exponential model of the equation: $\eta = k \cdot \dot{\gamma}^{(n-1)}$

Where k is the consistency index [N·s/m^2], and n is the flow behaviour index. The values of n determine the type of fluid, where:

n > 1 -> dilatant fluid
n = 1 -> Newtonian fluid
n < 1 -> pseudoplastic

In this case, n takes a value of -0.024, indicating a pseudo-plastic behaviour as indicated above.

Figure 6-2, Figure 6-3 and Figure 6-4 below show the behaviour versus time plots corresponding to the thixotropic model:

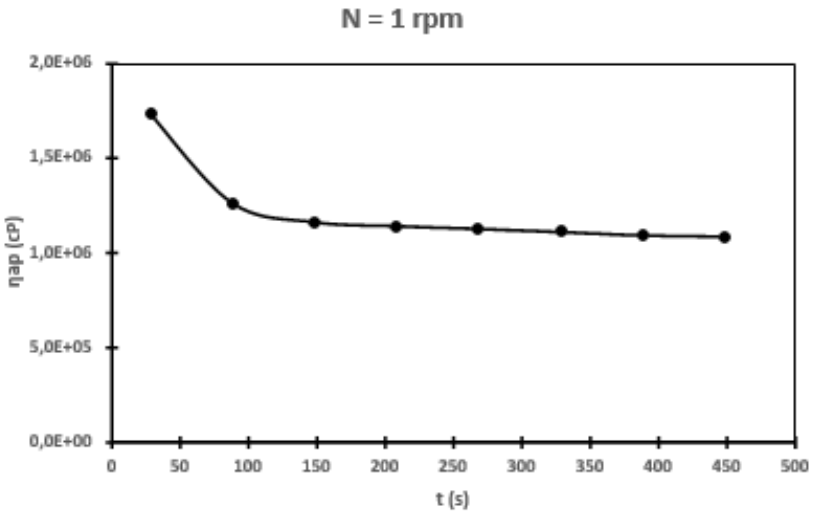

Figure 6-2. Behaviour thixotropic behaviour (N = 1 rpm)

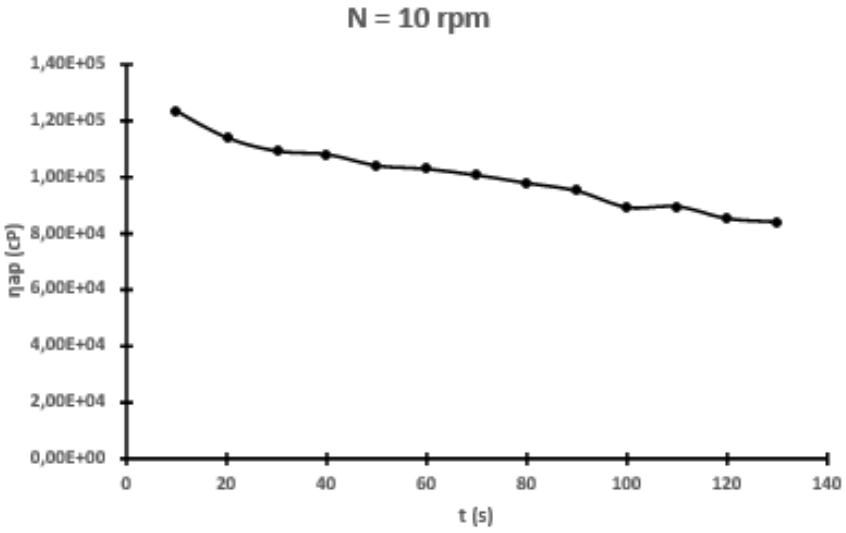

Figure 6-3. Thixotropic material behaviour (N = 10 rpm)

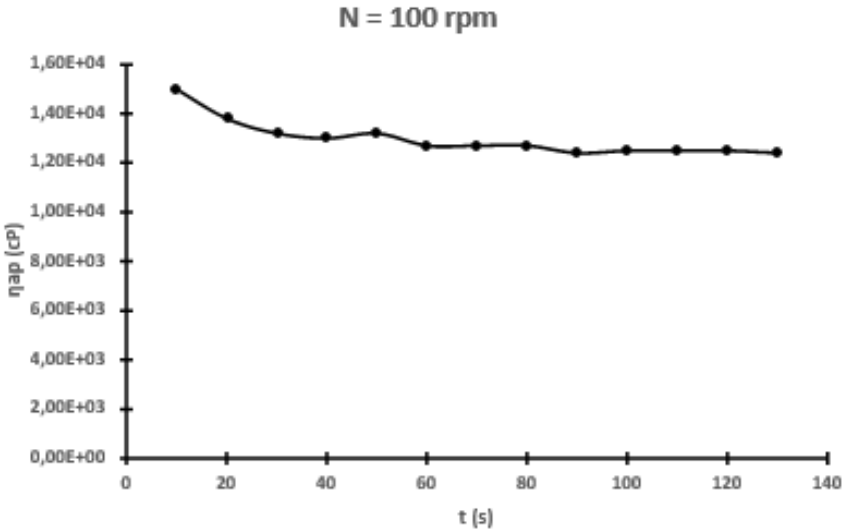

Figure 6-4. Thixotropic material behaviour (N = 100 rpm)

6.2 Description of the model

6.2.1 Description of the geometric model

The 3D geometric model is based on the test at the IDONIAL company facilities in the Roces Industrial Estate, Gijón lift tower (Asturias, Spain).

The test consisted of pumping the material through a pipe from ground level to a tank located on the roof of the building using a mobile pumping station with pressure regulation.

The pumping station is replaced in the simulation model by a cylinder of 144 mm diameter and length 400 mm where the pressure is applied as a boundary condition, see Figure 6-5. The pipe has a nominal diameter of 50 mm, corresponding to an NPS of 2 inches.

Different slope heights have been tested so that the length of the pipe varies between the different models, respecting the rest of the dimensions.

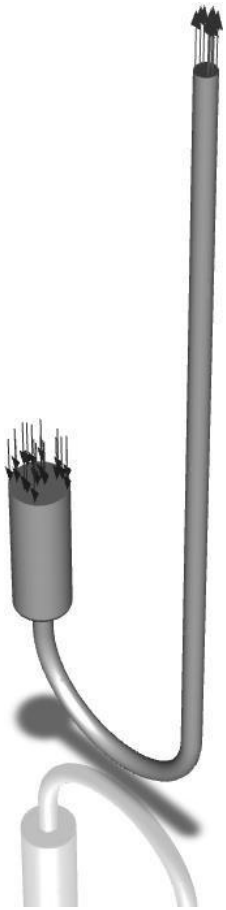

Figure 6-5. A geometric model for analysis

6.2.2 Description of the finite volume model

The finite volume model was developed based on the geometric model described in the previous subsection. This was generated using a structured mesh with hexahedral elements of 15 mm in length. Figure 6-6 presents a detail of the generated model. The number of elements varies depending on the case study, directly associated with the length of the pipe.

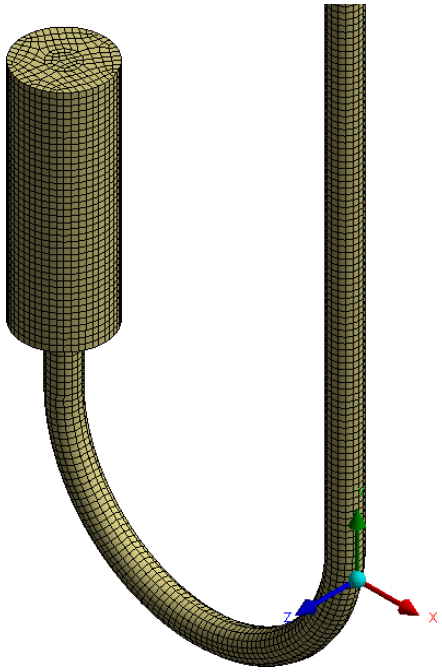

Figure 6-6. Detail of the mesh of the finite volume model

6.3 Boundary conditions

For the analysis of the model, the boundary conditions that allow the proposed installation to be simulated have been considered. At the inlet of the pipe, a pressure is introduced that simulates the pressure exerted by the pumping station on the fluid. A zero-gauge pressure is set at the outlet of the pipe, which simulates the outlet to 'free air' (atmospheric pressure). In both analyses, gravity considers the self-weight of the fluid under study.

6.3.1 Boundary conditions

The different boundary conditions used in the analyses are presented below:

- **Analysis 1. Pumping head.** A pressure sweep was carried out to obtain the fluid's different equilibrium heights. The pressure is introduced through a pressure inlet in the cylinder applied to the fluid. The outlet condition is set with a pressure outlet of zero value.
- **Analysis 2. Mass flow rate.** Different pipe lengths were used, varying the gradient from the ground-level pumping station to the maximum head. A sweep was carried out at different pressures for each length. Again, the pressure-inlet condition was used for fluid injection and zero pressure outlet for the outlet.

6.3.2 Time step

The simulations utilise transient analysis with a variable time step, keeping the Courant number constant and of value 0.2. The time intervals ranged from 0.001 s for the initial instants of the simulation to 1 s when reaching the equilibrium points.

6.4 Results of the fluid-dynamic analysis

The results obtained from the fluid-dynamic analyses for the described geometry and boundary conditions are presented below.

6.4.1 Pumping head

As mentioned in the previous section, a pressure sweep was applied to determine the equilibrium head in the pipe. These pressures start at 1x105 Pa and reach a maximum of 8x105 Pa, referred to as manometric values. The graph in Figure 6-7 represents the results obtained.

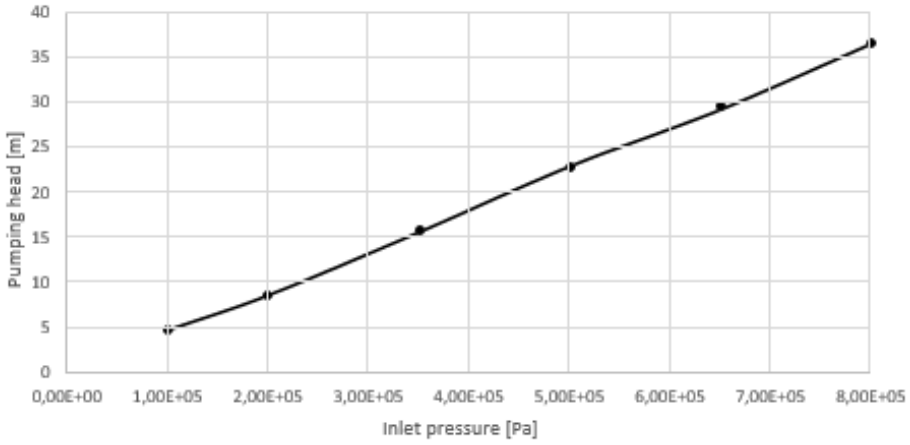

Figure 6-7. Maximum pumping head for different pressures

The results show a linear relationship between inlet pressure and maximum pumping head.

6.4.2 Mass flow rate

Utilising a pressure sweep, varying the length of the pipe and thus the height, the mass flow rate is obtained for the different combinations. The results are represented in the following graph in logarithmic scale, Figure 6-8.

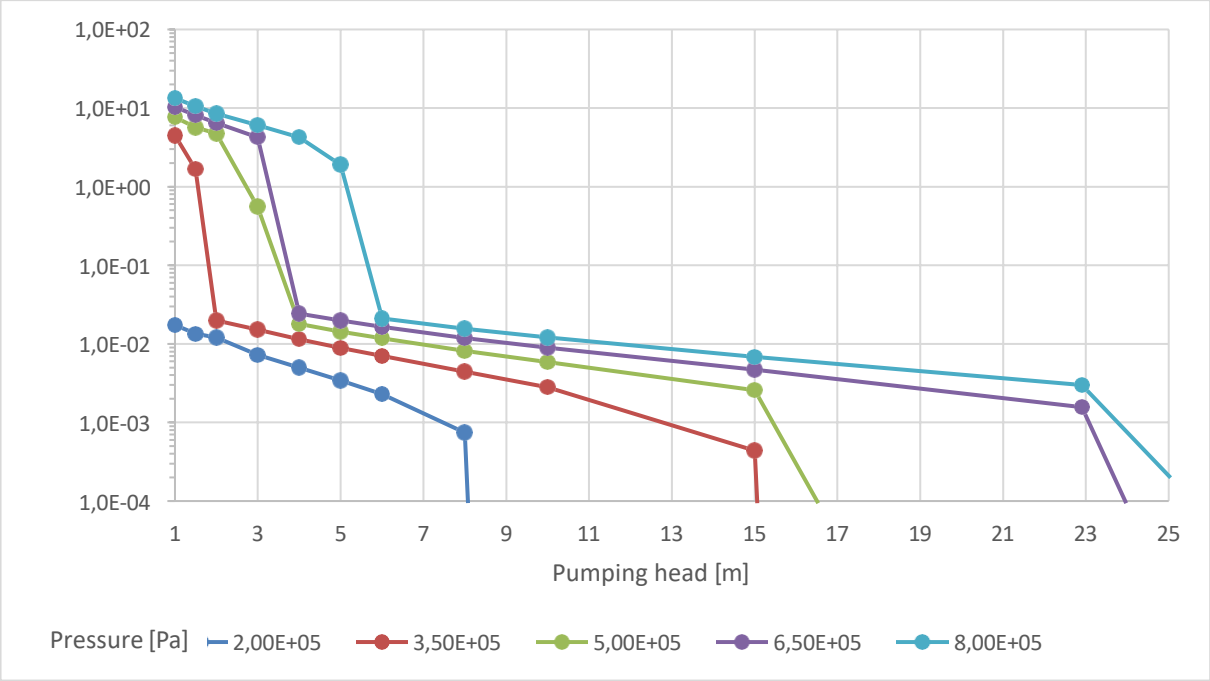

Figure 6-8. Mass flow rate for different pressures and heads

A logarithmic behaviour is observed for high flow rates. As the pumping head increases, there is a sharp decrease in flow rate up to about 0.02 kg/s in all cases. From that point on, it continues again with a logarithmic adjustment that continues up to a limit at zero, where the equilibrium pressure is reached. This behaviour could be related to the pseudo-plastic properties of the fluid.

7 Conclusions & lessons learnt

Hydropower is the preferred solution for large-scale energy storage as it is a mature technology that has been providing dispatchable power since the beginning of the electric era. With over 90% of the existing capacity, it will most likely remain at the top, at least where topographic conditions are good.

An essential consideration for conventional hydropower energy systems and pumped hydro storage is the footprint required by the reservoirs. Unconventional pumped hydro storage is directed to a small footprint pumped hydro energy storage system and method with high power output. The system uses a high-density fluid and allows for different configurations where upper and lower reservoirs may be at the same elevation. Hydraulic pumps and turbines may be placed higher than the lower reservoir, for example, on the surface above an underground mine.

A more compact pumped hydro energy storage system can be achieved by employing high-density fluid. For a given reservoir or tank volume, the energy storage capacity is proportional to the density of the fluid. For example, in the case where the high-density fluid has a density of 3x, the energy storage capacity of the system is 3 times that when water is used. This is because the mass flow rate is about 3 times more than water's.

Various types of slurry mixtures may be employed. The slurry mixture may include, for example, metal oxide particles mixed with a lower-density fluid, such as water. Other types of particles and lower-density fluids may also be helpful. The volume of particles in the slurry may equal or exceed 50%.

Two samples have been taken from company Hulleras del Norte S.A. S.M.E. (HUNOSA - Spain), one sample from company Węglokoks Kraj S.A. (WEGLO - Poland) and one sample from company Premogovnik Velenje d.o.o. (PV - Slovenia) to analyse the viability of developing slurry mixtures with material from waste heaps via rheometric tests specifically designed to obtain the stationary viscous response and linear viscoelastic response of the samples under study.

The lessons relevant to the Project from this deliverable can be summarised as follows:

1. A small surfactant (less than 1%) should be added to prevent the slurry from coalescing and improve flow. In some cases, antifreeze may be added to prevent freezing of the slurry. The concentration of antifreeze should be sufficient to prevent the slurry from freezing.

2. The reproducibility of the obtained rheometric results confirmed that the samples' homogeneity was achieved by shaking them manually for at least 5 minutes before starting the studies.

3. In all cases, in the viscous response and in the range of shear rates that were accessible (reproducible results), it is observed that viscosity decreases with increasing shear rate.

4. The viscoelastic study was carried out to determine the characteristic time of each sample (relaxation time), which gives an idea of the dominant behaviour (viscous or elastic) depending on the duration of the mechanical action exerted on the material behaviour (viscous or elastic) as a function of the duration of the mechanical action exerted on the material. This study is defined in the linear viscoelastic response region.

5. The results of the fluid-dynamic analysis, in conjunction with the rheology test data, show the pumping capabilities of the high-density fluid, particularly in the upward direction.

6. The dumpsite minerals from the mines are initially attractive as base materials for dense fluids. The samples from Slovenia and Spain show values in the interval bounded by our contrast formulations, which have already been used to prepare dense fluids. The sample for Poland is out of bounds but might also be helpful.

7. These results may serve as a reference in subsequent phases of the project, allowing the dimensioning of installations.

8 Glossary

AM – Ante Meridiem

E&M – Electrical and Mechanical

FAEN – Fundación Asturiana de la Energía

GW – Gigawatt

GWh – Gigawatt hour

HUNOSA – Hulleras del Norte, S.A.

m.a.s.l. – meters above sea level

M&B – Magellan & Barents

MW – Megawatt

MWh – Megawatt hour

OMIE – Operador del Mercado Ibérico de Electricidad

Solar PV – Solar Photovoltaics

UNIOVI – Universidad de Oviedo

USA – United States of America

References

Papers in journals:

Alvarado-Ancieta, C. (2009). Estimating E&M powerhouse cost. *Water Power Magazine.* https://www.waterpowermagazine.com/features/featureestimating-em-powerhouse-costs

Barnes, H.A., Carnalli, J.O. (1990). The vane-in-cup as a novel rheometer geometry for shear thinning and thixotropic materials, J. Rheol. 34, 841-866.

Bodis, K., Kougias, I., Taylor, N., & Jager-Waldau, A. (2019). Solar photovoltaic electricity generation: A lifeline for the European coal regions in transition. Sustainability 11(13), 3703. https://doi.org/10.3390/su11133703

Madlener, R., & Specht, J.M. (2020). An exploratory economic analysis of underground pumped-storage hydropower plants in abandoned deep coal mines. Energies 13(21), 5634. https://doi.org/10.3390/en13215634

McKinsey & Company (2022). Net-zero heat. Long Duration Energy Storage to accelerate energy system decarbonisation. LDES Council, November 2022. https://www.mckinsey.com/capabilities/sustainability/our-insights/net-zero-heat-long-duration-energy-storage-to-accelerate-energy-system-decarbonization#/ (accessed 25 November 2022).

Menendez, J., Ordonez, A., Alvarez, R., & Loredo, J. (2019). Energy from closed mines: Underground energy storage and geothermal applications. Renewable & Sustainable Energy Reviews 108, 498-512. https://doi.org/10.1016/j.rser.2019.04.007

Naranjo-Herrera, L.F., Páez-Flor, N.M., Rubio- Hernández, F.J. (2022). Using natural raw materials and CEM approach for the design of Andean volcanic self-compacting concretes, Processes 10, 1820.

Ortega, M., del Río, P., Ruiz, P., Nijs, W., & Politis, S. (2020). Analysing the influence of trade, technology learning and policy on the employment prospects of wind and solar energy deployment: The EU case. Renewable and Sustainable Energy Reviews 122, 109657. https://doi.org/10.1016/j.rser.2019.109657

Rodríguez-Huerta, E., Rosas-Casals, M., Sorman, A.H. (2017). A societal metabolism approach to job creation and renewable energy transitions in Catalonia. Energy Policy 108, 551-564. http://dx.doi.org/10.1016/j.enpol.2017.06.024

Rubio Hernández, F.J. (2020). Flujos no-Newtonianos y Reología, UMA Editorial, Universidad de Málaga, Málaga 2022

Temiz, M., & Javani, N. (2020). Design and analysis of a combined floating photovoltaic

system for electricity and hydrogen production. International Journal of Hydrogen Energy, 45(5), 3457-3496. https://doi.org/10.1016/j.ijhydene.2018.12.226

Viswanathan, V., Mongird, K., Franks, R., Li, X. Sprenkle, V., & Pacific Northwest National Laboratory (2022). 2022 Grid Energy Storage Technology Cost and Performance Assessment. Technical Report, Publication No. PNNL-33283, August 2022. U.S. Department of Energy: https://www.pnnl.gov/sites/default/files/media/file/ESGC%20Cost%20Performance%20Report%202022%20PNNL-33283.pdf (accessed 6 February 2023)

Reports & Legislation:

IEA (2022). *Renewables 2022. Analysis and forecasts to 2027.*. Copenhagen: European Environment Agency. Available on line: https://www.iea.org/reports/renewables-2022/executeve-summary (accessed 28 March 2023).

International Renewable Energy Agency (IRENA) (2018). Power System Flexibility for the Energy Transition: IRENA FlexTool methodology. Available on line: https://www.irena.org/-/media/Files/IRENA/Agency/Publication/2018/Nov/IRENA_Power_system_flexibility_2_2018.pdf?la=en&hash=B7028E2E169CF239269EC9695D53276E084A29A (accessed 28 March 2023).

Webpages:

Euenergy (2023). Electricity Prices of Europe. https://euenergy.live/

Hydrostor (2023). https://www.hydrostor.ca/

Nord Pool Price Data (2023). Day-ahead prices. https://www.nordpoolgroup.com/en/Market-data1/Dayahead/Area-Prices/ALL1/Hourly/?view=table

OMIE (2023). Operador del Mercado Ibérico de Electricidad. https://www.omie.es/

Pacific Northwest National Laboratory (2022). Energy Storage Cost and Performance Database. URL: https://www.pnnl.gov/ESGC-cost-performance (accessed 25 November 2022).

Pyhäsalmi (2023). https://www.epv.fi/en/project/a-pump-storage-station-for-pyhasalmi-mine/

Rhe Energy (2023). https://www.rheenergise.com/

Shell International (2023). https://patents.google.com/patent/US4691524

Relevant patents

Magellan & Barents S.L. (2022). US patent 11365713B2. http://www.patents.google.com/patent/US11365713B2/en?oq=Us+11%2c365713

Magellan & Barents S.L. (2022). China patent CN 112119213 B. http://epub.cnipa.gov.cn/cred/CN112119213B

WO 2019/202456 A1 (2019). "Pumped hydro energy storage system and method". 24 October 2019.

Appendix

Appendix 1. Experimental measurements of stationary viscosity.

FDPT1			
$\dot{\gamma}\ (1/s)$	$\eta_*\ (Pa \cdot s)$	$\eta_+\ (Pa \cdot s)$	$\eta_-\ (Pa \cdot s)$
50	0.718	0.6027	0.718
37.81	0.6563	0.6562	0.6563
28.59	0.7444	0.7347	0.7444
21.62	0.9106	0.9179	0.9106
16.35	1.204	1.198	1.204
12.37	1.576	1.558	1.576
9.35	2.057	1.991	2.057
7.071	2.671	2.705	2.671
5.348	3.379	3.404	3.379
4.044	4.468	4.544	4.468
3.058	6.811	5.925	6.811
2.313	7.395	7.718	7.395
1.748	10.15	9.972	10.15
1.322	12.77	14.27	12.77
1	17.31	17.6	17.31

FDPT1			
$\dot{\gamma}\ (1/s)$	$\eta_*\ (Pa \cdot s)$	$\eta_+\ (Pa \cdot s)$	$\eta_-\ (Pa \cdot s)$
50	0.4225	0.4266	0.4225
38.92	0.4353	0.4399	0.4353
30.3	0.4839	0.4907	0.4839
23.58	0.5696	0.5784	0.5696
18.36	0.6922	0.7028	0.6922
14.29	0.8477	0.8618	0.8477
11.12	1.042	1.059	1.042
8.658	1.283	1.304	1.283
6.739	1.584	1.611	1.584
5.246	1.964	1.997	1.964
4.084	2.444	2.484	2.444
3.179	3.052	3.103	3.052
2.474	3.824	3.888	3.824
1.926	4.805	4.886	4.805
1.499	6.051	6.15	6.051
1.167	7.639	7.768	7.639
0.9084	9.660	9.819	9.66
0.7071	12.23	12.45	12.23
0.5504	15.51	15.82	15.51
0.4285	19.7	20.02	19.7
0.3335	25.05	25.51	25.05
0.2596	31.88	32.41	31.88
0.2021	40.51	41.15	40.51
0.1573	51.45	52.34	51.45
0.1224	65.28	66.28	65.28
0,09531	82.8	84.36	82.8
0,07419	104.9	107.1	104.9
0.05775	133.1	135.5	133.1
0.04496	168.8	171.3	168.8
0.03499	213.3	217.4	213.3
0.02724	271.7	276.2	271.7
0.0212	346.1	353.9	346.1
0.01651	438.4	449.2	438.4
0.01285	556.8	569.3	556.8
0.01	704.7	724.1	704.7

FDBA			
$\dot{\gamma}\ (1/s)$	$\eta_*\ (Pa \cdot s)$	$\eta_+\ (Pa \cdot s)$	$\eta_{\_}\ (Pa \cdot s)$
100	0,8772	0,8499	0,8352
78,97	0,9692	0,9329	0,9106
62,35	1,143	1,096	1,066
49,24	1,377	1,32	1,283
38,88	1,659	1,593	1,55
30,7	1,999	1,923	1,873
24,24	2,413	2,326	2,269
19,14	2,921	2,821	2,755
15,12	3,551	3,437	3,358
11,94	4,338	4,203	4,111
9,427	5,319	5,155	5,049
7,444	6,543	6,343	6,22
5,878	8,076	7,833	7,682
4,642	9,99	9,705	9,514
3,665	12,38	12,04	11,8
2,894	15,38	14,96	14,67
2,285	19,13	18,63	18,27
1,805	23,82	23,22	22,77
1,425	29,67	28,97	28,39
1,125	36,95	36,21	35,44
0,8886	46,14	45,14	44,35
0,7017	57,63	56,37	55,41
0,5541	72,01	70,68	69,06
0,4375	89,98	89,12	86,58
0,3455	112,1	110,9	109,7
0,2729	141,9	138,8	137,3
0,2154	177	171,8	171,3
0,1702	223,2	219	216,6
0,1344	276,5	269,4	266,7
0,1061	347,2	337,9	336,9
0,08374	435,5	436,6	423,2
0,06622	541,8	528,1	527,9
0,05225	675,9	668,6	659
0,04127	838,9	808,6	803,4
0,03263	1047	1017	1002
0,02569	1342	1230	1277
0,02033	1692	1579	1590
0,01608	2130	2007	2012
0,01269	2692	2561	2536
0,009993	3452	3221	3246

FDPT2			
$\dot{\gamma}\ (1/s)$	$\eta_*\ (Pa \cdot s)$	$\eta_+\ (Pa \cdot s)$	$\eta_{\_}\ (Pa \cdot s)$
100	1,261	1,144	1,134
78,97	1,491	1,375	1,37
62,35	1,822	1,7	1,71
49,24	2,239	2,09	2,079
38,88	2,756	2,57	2,581
30,7	3,374	3,169	3,196
24,24	4,153	3,899	3,948
19,14	5,122	4,786	4,874
15,12	6,315	5,892	6,033
11,94	7,788	7,28	7,434
9,427	9,609	9,013	9,18
7,444	11,87	11,14	11,32
5,878	14,64	13,79	14,03
4,642	18,12	17,06	17,35
3,665	22,45	21,11	21,44
2,894	27,84	26	26,61
2,285	34,56	32,07	33,05
1,805	42,92	39,61	41,07
1,425	53,31	49,1	51,07
1,125	66,31	60,94	63,46
0,8887	82,31	75,56	78,88
0,7018	102,1	93,61	98,18
0,5542	126,9	116	121,8
0,4376	157,5	143,5	150,6
0,3456	194,4	177,5	186,8
0,273	240,7	219	229,9
0,2155	297,4	271,1	283,4
0,1702	367,9	334	346,7
0,1344	455,1	414,5	423,8
0,1061	558,4	504,9	523,9
0,08389	684,5	620,6	633,6
0,06619	851,3	764,7	790,2
0,05231	1047	941,1	963,4
0,04129	1288	1162	1189
0,03258	1596	1421	1492
0,02568	2016	1750	1844
0,02034	2526	2189	2274
0,01608	3099	2725	2847
0,01271	3807	3421	3588
0,01001	4758	4305	4514

FDPO			
$\dot{\gamma}\ (1/s)$	$\eta_*\ (Pa \cdot s)$	$\eta_+\ (Pa \cdot s)$	$\eta_-\ (Pa \cdot s)$
100	0,264	0,2642	0,2621
78,97	0,2076	0,2045	0,2042
62,35	0,19	0,1868	0,1847
49,24	0,189	0,1856	0,1833
38,88	0,1928	0,189	0,1863
30,7	0,1973	0,1949	0,1933
24,24	0,1888	0,1871	0,1854
19,14	0,1929	0,1915	0,1867
15,12	0,227	0,2209	0,2168
11,94	0,2794	0,2721	0,2671
9,427	0,3491	0,3396	0,334
7,444	0,4356	0,4241	0,4172
5,878	0,5432	0,5291	0,5206
4,642	0,6742	0,6573	0,6472
3,665	0,8404	0,8185	0,807
2,894	1,047	1,022	1,009
2,285	1,311	1,278	1,264
1,805	1,644	1,603	1,584
1,425	2,065	2,013	1,992
1,125	2,59	2,531	2,52
0,8886	3,257	3,185	3,181
0,7017	4,124	4,04	4,019
0,5541	5,218	5,107	5,093
0,4375	6,592	6,437	6,461
0,3455	8,308	8,13	8,193
0,2728	10,48	10,25	10,39
0,2154	13,3	13,04	13,24
0,1701	16,91	16,61	16,87
0,1343	21,47	21,11	21,6
0,1061	27,33	26,87	27,48
0,08377	34,91	34,15	35,2
0,06615	44,35	43,4	44,84
0,05223	56,37	55,38	56,9
0,04125	71,91	70,46	72,76
0,03257	90,86	89,81	92,82
0,02572	116,1	114,1	118,9
0,02031	147,2	146,2	150,7
0,01604	187,3	186,7	194,6
0,01266	240,4	238,7	250,1
0,01	309,3	306	318,9

FDESL			
$\dot{\gamma}\ (1/s)$	$\eta_*\ (Pa \cdot s)$	$\eta_+\ (Pa \cdot s)$	$\eta_-\ (Pa \cdot s)$
100	0,5844	0,5938	0,6002
78,97	0,5791	0,5897	0,5962
62,35	0,5683	0,5774	0,5836
49,24	0,5657	0,5777	0,5868
38,88	0,6242	0,6331	0,6459
30,7	0,7256	0,7505	0,7689
24,24	0,8999	0,9289	0,9513
19,14	1,104	1,137	1,161
15,12	1,339	1,373	1,4
11,94	1,621	1,66	1,694
9,427	1,968	2,013	2,054
7,444	2,394	2,451	2,501
5,878	2,93	2,995	3,057
4,642	3,595	3,673	3,75
3,665	4,43	4,52	4,611
2,894	5,463	5,578	5,688
2,285	6,752	6,896	7,024
1,805	8,366	8,516	8,683
1,425	10,36	10,56	10,75
1,125	12,87	13,13	13,34
0,8886	16,03	16,35	16,61
0,7017	19,93	20,4	20,72
0,5541	24,9	25,49	25,91
0,4376	31,24	31,83	32,49
0,3455	39,19	39,84	40,65
0,2729	49,03	50,04	51,01
0,2154	61,87	62,75	64,08
0,1701	78,48	79,47	80,98
0,1343	98,63	100,2	102,5
0,1061	121,5	126,2	129,9
0,0838	143,9	144,7	163,8
0,06615	172,1	170,6	187,8
0,05226	208,8	209,5	225
0,04124	259,8	265	281,4
0,03259	319,7	324,8	348,1
0,02573	406,8	415	429,8
0,0203	527,8	534,4	550,4
0,01603	663	682,7	715,5
0,01267	851,2	860,3	928,3
0,009993	1094	1125	1194

Appendix 2. Experimental measurements corresponding to the amplitude sweeps

FDMA						
$\gamma_{\&}(-)$	$G'_{*}(Pa)$	$G''_{*}(Pa)$	$G'_{+}(Pa)$	$G''_{+}(Pa)$	$G'_{\_}(Pa)$	$G''_{\_}(Pa)$
0.00009608	1947	490.3	1977	491.2	1971	479.1
0.0001311	1915	499.6	1903	511.5	1962	522.7
0.0001704	1852	493.7	1854	504.1	1862	507.1
0.0002215	1787	490.7	1799	498	1860	505.8
0.000282	1727	495.7	1728	499.2	1770	514.8
0.0003603	1635	494	1631	496.6	1540	465.4
0.0004599	1504	479.5	1495	478.1	1456	452.8
0.0005869	1365	457.7	1355	454.3	1359	454.6
0.0007489	1221	436	1226	436.4	1229	438.1
0.0009557	1079	409.5	1084	412.7	1095	417.6
0.001218	939.2	382	942.4	384.9	946.8	392.4
0.001553	806.3	350.6	811.4	355.1	817.2	352.4
0.00198	682.4	319.3	686.8	322.1	686.6	318
0.002521	570.6	285.7	571.2	289.3	576.7	289.9
0.003211	468.2	252.8	468	255.2	474.2	256.4
0.003948	367,1	217.2	373.2	222	377.8	223
0.005206	283.5	189.7	285.1	191.3	288.6	192.9
0.006626	207.9	162.4	203.3	161.9	210	164.4
0.008422	154.3	139.4	152.1	139	154.9	140.1
0.01072	120.2	121	120.2	121.5	119.6	121.1

FDPO						
$\gamma_{\&}$ (–)	G'^{*} (Pa)	G''^{*} (Pa)	G'_{+} (Pa)	G''_{+} (Pa)	G'_{-} (Pa)	G''_{-} (Pa)
0,0001054	147,1	20,09	154,7	21,49	154,2	21,66
0,000148	165,8	19,27	168,8	20,52	172,1	20,85
0,000199	174,9	19,9	177,7	20,35	181,7	21,4
0,0002667	178,7	20,62	183,1	21,12	187,3	22,3
0,0003573	181,6	21,3	186,6	21,91	191,1	22,73
0,000474	184,3	22,16	187,4	22,3	193	23,37
0,0006315	184	22,41	186,9	23,58	192,4	24,44
0,0008432	181,3	24,34	185,1	25	189,8	26,22
0,001062	178,5	25,57	180,5	26,62	185,9	27,85
0,001493	171,6	27,83	173,8	28,53	178,2	30,09
0,00198	162,8	29,87	164,2	30,94	168,1	32,28
0,002654	150,9	32,12	151,4	33,14	154,6	34,53
0,003555	134,7	33,95	135,4	34,81	138,2	36,29
0,004745	120	35,08	120,6	35,98	122,9	37,32
0,006329	104,7	35,87	105,2	36,71	108,8	37,62
0,008442	88,99	35,99	89,28	36,79	91,38	38,09
0,01127	73,32	35,2	73,43	35,95	74,38	37,04
0,01502	58,3	33,41	58,09	34,06	58,44	34,91
0,01999	44,63	30,63	44,12	31,04	43,6	31,82
0,0266	33,35	27,02	31,83	27,6	31,33	28,16
0,03343	23,51	22,78	22,24	23,67	22,02	24,04
0,04699	16,11	19,09	15,72	20,03	15,66	20,27
0,0628	11,23	15,96	11	16,49	11,22	16,85
0,08308	7,91	13,26	7,81	13,58	8,049	13,95
0,1052	5,513	11,01	5,509	11,27	5,58	11,44

FDPT1						
$\gamma_{\&}$ (–)	G'_* (Pa)	G''_* (Pa)	G'_+ (Pa)	G''_+ (Pa)	G'_- (Pa)	G''_- (Pa)
8,827E-06	2333	181,1	2316	343,3	2283	482,6
7,472E-06	2474	1179	3116	1998	3168	1859
0,00001393	4473	3334	4319	2595	4233	2408
0,00001873	5402	3462	4537	2385	4385	2200
0,00002492	5571	3154	4864	2454	4814	2305
0,00003356	5497	2820	4930	2326	4649	2126
0,00004291	5569	2762	4659	2105	4546	1930
0,00005468	5273	2516	4475	2050	4358	1876
0,00007282	4709	2091	4078	1761	3963	1721
0,00009712	4332	2106	3599	1657	3550	1599
0,0001334	3672	1809	3194	1481	2971	1325
0,0001756	3108	1500	2749	1340	2656	1246
0,0002144	2717	1415	2352	1174	2283	1136
0,0003037	2171	1133	1973	1012	1923	1004
0,0003064	1795	1037	1745	944,8	1609	904,9
0,0003961	1452	903,7	1196	774,1	1327	777,5
0,00048	1212	788,2	1107	700,3	1109	689,1
0,0006252	799,3	639,4	795,8	616,3	826,2	604,8
0,0007383	761	585,8	703,7	586,7	679,3	631,7
0,001016	640,7	629,1	594,5	591,2	576,1	585,6

FDESL						
$\gamma_{\&}$ (–)	G'_* (Pa)	G''_* (Pa)	G'_+ (Pa)	G''_+ (Pa)	G'_- (Pa)	G''_- (Pa)
0,0002227	1149	807	1380	873,1	1265	1063
0,0003377	1380	847,3	1555	877,5	1463	955,5
0,0004785	1351	849,7	1462	863,3	1504	907
0,0006175	1282	823,8	1385	837,1	1381	824,7
0,0007516	1237	794,1	1239	787,6	1224	766,3
0,0009666	1095	737,9	1149	742,1	1115	714,9
0,001233	944,2	671,4	987,5	674,1	937,8	641,4
0,001569	792,6	597,7	822,1	595,8	789,4	571,4
0,001996	652,8	519,2	693,4	524	640,2	493,5
0,002534	530	443,4	568,4	450,5	512,2	418,1
0,003221	424,4	372,3	455,4	379,8	414	352,8
0,004094	337,1	310,7	372,4	319,9	329,5	295,7
0,005205	264,1	257,3	301,6	269	260,6	247
0,006621	204,7	213,1	241,8	227,4	205,3	206,6
0,008422	158	177,4	192,2	192,9	161,3	174,2
0,01072	122,2	149,7	152,2	165,3	115,1	142,2

FDPT2						
$\gamma_{\&}$ (–)	G'_{*} (Pa)	G''_{*} (Pa)	G'_{+} (Pa)	G''_{+} (Pa)	$G'_{\_}$ (Pa)	$G''_{\_}$ (Pa)
0,00008917	13110	7277	7505	8253	12890	7061
0,0001521	14270	4638	13920	4583	13760	4345
0,0002514	14620	3754	14250	3691	14170	3617
0,0004301	14090	3174	13890	3182	13510	3027
0,0006938	13280	2965	13020	2902	12970	2926
0,001128	12160	2835	11940	2765	11750	2735
0,00185	10300	2653	10230	2612	9707	2507
0,003038	8836	2571	8407	2467	8662	2454
0,004435	5692	2012	6834	2286	6496	2170
0,00849	4908	1870	4966	1913	5076	1953
0,01274	3516	1590	3429	1597	3388	1551
0,02545	2451	1367	2236	1273	2413	1352
0,0374	1810	1176	1747	1132	1784	1160
0,05632	1116	916,4	1259	967,2	1232	955,8
0,08596	792,5	781,1	784,1	773,9	739,7	747
0,1412	485,8	622,3	480,6	613,9	378,5	495,1
0,2321	251,8	453,7	240,9	434,4	223,9	410,9
0,3819	121,2	383,3	117,9	376,4	120,8	376,6
0,6027	47,67	370,4	42,95	360,7	26,41	300,9
0,7118	31,07	298,5	26,82	290,7	27,58	286,4

FDBA						
$\gamma_{\&}$ (–)	G'_* (Pa)	G''_* (Pa)	G'_+ (Pa)	G''_+ (Pa)	$G'_{\_}$ (Pa)	$G''_{\_}$ (Pa)
0,00001528	785,8	1313	706	1157	746,7	909,8
0,00001037	106,7	2230	44,63	1321	76,32	1871
0,00001362	9075	12250	4651	10690	9019	12190
0,00003354	18560	8861	18450	8556	18320	8636
0,00006761	18150	6035	17570	6234	18650	6373
0,0001028	17860	5335	17470	5424	17850	5057
0,0001788	15010	4282	14530	4340	15620	4381
0,0002952	12650	3813	12440	3714	13100	3884
0,0004419	7212	2634	9183	3220	7916	2760
0,0007701	6558	2324	6185	2538	6340	2380
0,001062	3223	1422	4951	2166	8488	2991
0,00204	2845	1255	2487	1310	4411	1625
0,003624	1809	1014	2305	1153	1724	826
0,004754	1498	797,2	1574	831,4	1389	632,3
0,009877	905,1	534	1085	623,2	981,7	512,2
0,01559	627,2	409,8	707,3	464,1	661,6	403,4
0,0248	403,3	312,5	411,7	325,2	420,7	315,3
0,03953	244,3	234	244,9	236,7	252,9	239,9
0,06323	149,8	176,5	149,8	177,8	142,7	172,3
0,1017	102,3	139,6	102,8	140,6	103,2	142,6
0,1642	74,19	114,6	75,17	116,2	75,84	118,4
0,2654	54,6	98,2	55,92	100,1	55,06	99,63
0,4291	40,77	86,66	45,3	92,1	40,46	86,91
0,6928	25,55	69,79	27,44	73,15	25,4	70
1,058	14,69	53,16	14,43	53,27	13,46	50,9

Appendix 3. Experimental measurements corresponding to the frequency sweeps

FDMA						
$f\ (Hz)$	$G'_*\ (Pa)$	$G''_*\ (Pa)$	$G'_+(Pa)$	$G''_+(Pa)$	$G'_{,}\ (Pa)$	$G''_{,}\ (Pa)$
0,1	1666	733,2	1526	744,4	1666	733,2
0,0631	1672	859,4	1635	896,2	1672	859,4
0,03981	1554	980,5	1573	1041	1554	980,5
0,02512	1289	1066	1323	1143	1289	1066
0,01585	1049	1111	1167	1249	1049	1111
0,01	959	1209	1080	1387	959	1209

FDPT1						
$f\ (Hz)$	$G'_*\ (Pa)$	$G''_*\ (Pa)$	$G'_+(Pa)$	$G''_+(Pa)$	$G'_{,}\ (Pa)$	$G''_{,}\ (Pa)$
10	3449	1741	3507	1735	3394	1691
6,31	3360	2220	3409	2116	3224	2262
3,981	3001	2296	3061	2166	2875	2138
2,512	2392	2541	2533	2464	2450	2459
1,585	1276	2321	1735	2677	1427	2425
1	367,7	1420	682,6	1925	518,6	1626

FDPO						
$f\ (Hz)$	$G'^*\ (Pa)$	$G''^*\ (Pa)$	$G'+\ (Pa)$	$G''+\ (Pa)$	$G',(Pa)$	$G'',(Pa)$
0,00631	153,9	115,7	154,9	114,7	152,9	116,7
0,003981	235,8	210,2	232,8	208,2	231,8	207,2
0,002512	325,2	319,6	330,2	319,6	332,2	317,6
0,001585	434	450	404	450	414	460

FDESL						
$f\ (Hz)$	$G'_*\ (Pa)$	$G''_*\ (Pa)$	$G'_+(Pa)$	$G''_+(Pa)$	$G'_{,}\ (Pa)$	$G''_{,}\ (Pa)$
0,3981	2710	2005	2720	2010	2725	2005
0,2512	2845	2156	2835	2146	2825	2136
0,1585	3050	2582	3050	2592	3055	2582
0,1	3093	3168	3083	3178	3063	3188
0,0631	3173	3971	3183	3991	3163	3961

FDPT2						
$f\ (Hz)$	$G'_*\ (Pa)$	$G''_*\ (Pa)$	$G'_+(Pa)$	$G''_+(Pa)$	$G'_-\ (Pa)$	$G''_-\ (Pa)$
0,1	10730	4149	10720	4249	11720	4149
0,0631	12190	4059	12290	4159	12290	4179
0,03981	13200	3979	13100	3979	12100	3999
0,02512	14170	4126	14190	4126	13190	4226
0,01585	14920	4318	14720	4218	14720	4218
0,01	15230	3784	15250	3884	15250	3984
0,00631	15280	4081	15380	4081	15580	4081
0,003981	15330	4358	15230	4158	15230	4188
0,002512	15310	4473	15380	4273	15580	4263
0,001585	15360	4376	15460	4376	15460	4176

FDBA						
$f\ (Hz)$	$G'_*\ (Pa)$	$G''*\ (Pa)$	$G'_+(Pa)$	$G''_+(Pa)$	$G'_-\ (Pa)$	$G''_-\ (Pa)$
10	17390	5752	17490	5752	17590	4752
6,31	17760	5148	17760	5348	17860	5348
3,981	17430	4721	17450	4721	17430	4721
2,512	16940	4853	16940	4953	16940	4953
1,585	17140	5340	17240	5340	17340	5340
1	16640	5837	16640	5837	16640	5867
0,631	16570	6226	16670	6426	16570	6226
0,3981	16790	7100	16790	7100	16490	7500
0,2512	16140	7757	16180	7757	16140	7757
0,1585	15230	8288	15230	8388	15230	8188
0,1	15180	8396	15380	8396	15280	8396
0,0631	14720	9018	14720	9018	14720	9418
0,03981	13430	9683	13530	9883	14430	9583
0,02512	13880	10140	13780	10040	13880	10340
0,01585	13520	10440	13920	10340	13620	10240